Article

A Study on the Surface Properties of Ceria-Supported Tungsten and Copper Oxides

Lin Dong, Yuhai Hu, Fei Xu, Din Lu, Bin Xu, Zheng Hu, and Yi Chen

J. Phys. Chem. B, **2000**, 104 (1), 78-85• DOI: 10.1021/jp9914424 • Publication Date (Web): 16 December 1999

A Study on the Surface Properties of Ceria-Supported Tungsten and Copper Oxides

Lin Dong, Yuhai Hu, Fei Xu, Din Lu, Bin Xu, Zheng Hu, and Yi Chen*

Department of Chemistry, Institute of Mesoscopic Solid State Chemistry, Nanjing University, Nanjing 210093, China

Received: May 3, 1999; In Final Form: August 6, 1999

Laser Raman spectroscopy (LRS), Fourier transform infrared spectroscopy (FT-IR), X-ray diffraction (XRD), X-ray photoelectron spectroscopy (XPS), ultraviolet and visible diffuse reflectance spectroscopy (UV-DRS), and temperature-programmed reduction (TPR) are used to characterize a series of WO_3/CeO_2 samples. The results indicate that the dispersion capacity of tungsten oxide is about $4.8W^{6+}$ ions $nm^{-2}(CeO_2)$ and the structure of the supported tungsten oxide species is closely related to its loading amount on ceria. For the calcined samples, two distinctly different tungsten species have been identified by various methods. At low WO_3 loading, only the highly dispersed tungsten oxide species are found on the surface possibly formed by the incorporation of the dispersed W^{6+} ions into the surface vacant sites of CeO_2. Increasing the loading amount of tungsten oxide to a value above $4.8W^{6+}$ ions $nm^{-2}(CeO_2)$ leads to the formation of crystalline WO_3. LRS and IR results of WO_3/CeO_2 samples prepared by using different precursors have shown that calcination has a dramatic effect on the structure of the final product, which might mostly eliminate the differences of the precursors and result in final products with almost a same structure. TPR results of WO_3/CeO_2, CuO/CeO_2, and CuO/WO_3-CeO_2 samples reveal that the reduction behaviors of CuO dispersed on CeO_2 and on WO_3 premodified CeO_2, i.e., WO_3-CeO_2, are apparently different. The result emphasizes the importance of the surface structure of the support on the properties of the dispersed metal oxide species; the conclusion is also supported by UV-DRS results. The coordination environments of the dispersed tungsten oxide and copper oxide species are discussed on the basis of the incorporation model (Chen, Y.; Zhang, L. *Catal. Lett.* **1992**, *12*, 51).

Introduction

Supported metal oxides are extensively used as heterogeneous catalysts in numerous chemical processes, e.g., ranging from hydrodesulfurization, cracking, polymerization, and partial oxidation of hydrocarbons to the selective reduction of nitrogen oxides. Many studies have been focused on the preparation, characterization, and catalytic properties of the catalysts. It is known that the properties of the supported metal oxide species are often different from those of the pure metal oxide. Various views concerning the nature of the interactions between metal oxide and support have been reviewed in the literature.[1−5] It is well established that, even for a same metal oxide−support system, the supported metal oxide species might have a variety of structures strongly depending on the experimental conditions such as the loading amount of the oxide and the calcination temperature, etc. For example, it has been argued that on γ-alumina molybdenum oxide might exist as (1) a monolayer of isolated tetrahedrally coordinated units, (2) a monolayer of octahedrally coordinated and/or polymeric units, (3) surface species consisting of bi- and trilayer structures of the molybdenum oxide, or (4) bulk phase crystallites.[6] In addition, the formation of nonstoicheometric (two-dimensional) surface compounds through the interactions of metal oxide and support have also been suggested.[7] As mentioned by Massoth[6] and Chianelli et al.,[8] the commonly used techniques in characterizing these systems might cause some confusion. It is not surprising to see that, despite considerable efforts being devoted to this aspect, different explanations on the structure of dispersed oxide species and on the interactions between them and support can often be found in the literature.[1−8]

Knowledge of the local structure of the catalyst surface and of factors that determine the surface structure has played an important role in developing and optimizing supported metal oxide systems in heterogeneous catalysis. Characterization of the surface structure of supported metal oxides, however, is complicated since several different structures as well as chemical states might coexist in the supported metal oxide systems.[8−12] Thus, a good characterization technique should be effective in discriminating the different coexisting states. To date, the characterization techniques that can provide important information at the molecular or atomic level are available, e.g., extended X-ray absorption fine structure (EXAFS), X-ray absorption near edge spectroscopy (XANES), laser raman spectroscopy (LRS), Fourier transform infrared spectroscopy (FT-IR), and ultraviolet and visible diffuse reflectance spectroscopy (UV-DRS), etc. Each of these methods has its own specialty as well as limitation; applying them in compensative ways has been very helpful and popular.

Ceria, copper oxide, and tungsten oxide are important components in automotive exhaust emission control and industrial catalysts. For example, ceria and CeO_2-containing materials have been studied as key components in three-way catalysts (TWC) for treatment of exhaust gas from automobiles,[13] copper oxide has been demonstrated to be a very active species among the base-metal oxides for carbon monoxidation,[14] and the supported WO_3 catalysts are widely used in metathesis and hydrodesulfurization (HDS).[15,16] Studies on the properties of supported metal oxides and the interactions between the

10.1021/jp9914424 CCC: $19.00
Published on Web 12/16/1999

dispersed metal oxide species and supports would be helpful for our understanding of the catalytic behaviors. Since WO_3 and MoO_3 are chemically closely related, it seems reasonable to expect that when they are dispersed on the same support, respectively, the supported oxide systems should exhibit similar structural features. It is generally accepted that Mo exists in a highly dispersed monolayer-type structure on ceria and γ-alumina, although the exact identity of its structure is still open for discussion.[4,5,12,17−19] Comparatively, the supported WO_3/CeO_2 system has received little attention in the past. The purpose of this work is attempting to (1) determine the dispersion capacity of tungsten oxide supported on ceria, (2) reveal the effect of calcination on the formation of dispersed metal oxide species and correlate the structure of the surface tungsten oxide species to the characteristic Raman and IR bands with the help of the incorporation model,[20] and (3) explore the importance of surface structure of the support on the properties of the dispersed oxide by studying the different reduction behaviors of CuO supported on CeO_2 and on tungsten oxide premodified CeO_2 supports.

Experimental Section

I. Instrument. XRD patterns were obtained with a Shimadzu XD-3A diffraction meter employing Ni-filtered Cu Kα radiation (0.15418 nm). The X-ray tube was operated at 35 kV and 20 mA. The amount of bulk WO_3 was determined by XRD quantitative analysis as reported elsewhere[4] using α-alumina powder as reference.

XPS results were recorded with a V/G. Escalab MK II system equipped with a hemispherical electron energy analyzer. The spectrometer was operated at 15 kV and 20 mA, and an aluminum anode (Al Kα = 1486.6 eV) was used. The C_{1s} signal (285 eV) was taken as the reference to calculate the binding energies (BE).

Laser Raman spectra were recorded on a Bruker RFS-100 Fourier transform spectrometer with an InGaAs detector cooled by liquid nitrogen. Raman excitation at 1064 nm was provided by a Nd:YAG laser. The laser power measured at the powder sample ($\sim$30 mg) was 100 mW, and spectra were accumulated for 50 scans at 4 cm^{-1} resolution in backscattering geometry.

All the FT-IR spectra were taken with a Nicolet 510P Fourier transform infrared spectrometer operated with a spectral resolution of 4 cm^{-1}. Samples were pressed into self-supporting wafers ($\sim 25 \pm 2$ mg cm^{-2}) and placed into an IR cell equipped with CaF_2 windows in the atomosphere.

UV-DRS profiles were recorded in the range of 200−800 nm by a Shimadzu UV-240 spectrophotometer with a $BaSO_4$ sample as reference.

Temperature-programmed reduction (TPR) was carried out in a quartz U-tube reactor, and a 30 mg sample was used for each measurement. Prior to the reduction, the sample was pretreated in a N_2 stream at 373 K for 1 h and then cooled to room temperature. After that, a H_2-N_2 mixture (5% H_2 by volume) was switched on and the temperature was increased linearly at a rate of 10 K min^{-1}. The consumption of H_2 in the reactant stream was detected by a thermal conductivity cell.

II. Catalyst Preparation. CeO_2 support with a BET surface area of 75m^2 g^{-1} was prepared as described elsewhere.[21]

WO_3/CeO_2 samples were prepared by impregnating ceria with solutions containing various precursors, i.e., (1) aqueous solution of ammonium metatungstate $[(NH_4)_6H_2W_{12}O_{40}]$ at pH = 3, (2) aqueous solution of ammonium metatungstate $[(NH_4)_6H_2W_{12}O_{40}]$ at pH = 9, and (3) aqueous solution of $(NH_4)_2WO_2S_2$ (it was taken as a tungsten-containing compound for the formation of tungsten oxide species after calcination) at pH = 9, followed by drying at 373 K for 10 h and then calcining in flowing air at 773 K for 2 h.

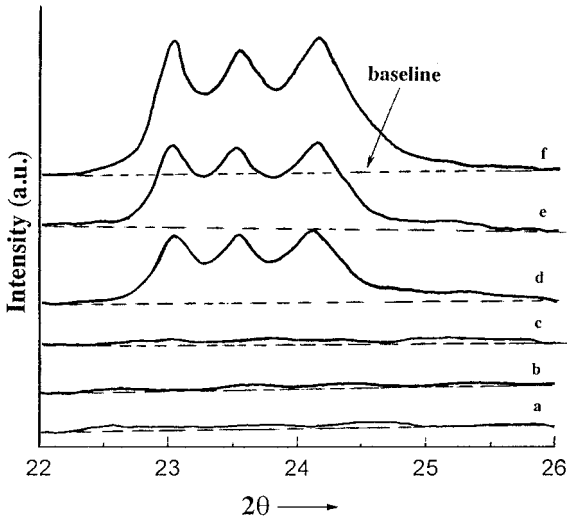

Figure 1. XRD patterns: (a) CeO_2; (b, c, and d) WO_3/CeO_2 samples with WO_3 loading of 1.2, 4.0, and 6.0 W^{6+} ions $nm^{-2}(CeO_2)$, respectively; (e) a mechanical mixture of WO_3 and CeO_2 (3.0 W^{6+} ions $nm^{-2}(CeO_2)$); (f) WO_3.

Results and Discussion

I. Dispersion of Tungsten Oxide on Ceria. All the WO_3/CeO_2 samples discussed in this section were prepared by impregnating the CeO_2 support with aqueous solutions containing the required amount of ammonium metatungstate $[(NH_4)_6H_2W_{12}O_{40}]$ at pH = 3, and this was followed by drying and calcining of appropriate concentrations as mentioned above.

Figure 1 shows the XRD patterns of a series of WO_3/CeO_2 samples with different WO_3 loadings. To identify the dispersion states of tungsten oxide in samples as prepared, the XRD patterns of a mechanical mixture of crystalline WO_3 and CeO_2 (with WO_3 around 3.0 W^{6+} ions $nm^{-2}(CeO_2)$) (e) as well as a WO_3 sample (f) are also presented for comparison. For samples with low WO_3 loading, i.e., (b) and (c) with 1.2 and 4.0 W^{6+} ions $nm^{-2}(CeO_2)$, respectively, no characteristic peaks of crystalline WO_3 (typically with $2\theta = 23.14°$, 23.64°, and 24.36° as shown in pattern f) has been observed. However, the characteristic peaks of bulk WO_3 can clearly be seen in sample d that has a loading of 6.0 W^{6+} ions $nm^{-2}(CeO_2)$. As shown in patterns e and f, the crystalline peaks of tungsten oxide can clearly be seen in these samples. The results demonstrate that tungsten oxide exists as highly dispersed surface species in low loading samples and crystalline WO_3 appears only in samples of high loading.

Figure 2 shows the amount of the crystalline WO_3 versus total tungsten oxide content in a series of WO_3/CeO_2 samples measured by XRD quantitative analysis. One can see that there is no crystalline WO_3 phase in samples with low WO_3 loading, and the straight line representing the formation of crystalline WO_3 does not go through the origin but gives an intercept on the abscissa at a value referred to as the dispersion capacity. Obviously, the dispersion capacity of a metal oxide is a critical value, at values lower than which the oxide might become highly dispersed on the support without the formation of its crystalline phase. The above results have shown that the dispersion capacity of tungsten oxide on CeO_2 is about 4.8W^{6+} ions $nm^{-2}(CeO_2)$.

As listed in Table 1, the binding energies of $W4f_{5/2,7/2}$, and $Ce3d_{5/2}$ of the WO_3/CeO_2 samples are around 37.7, 35.7, and

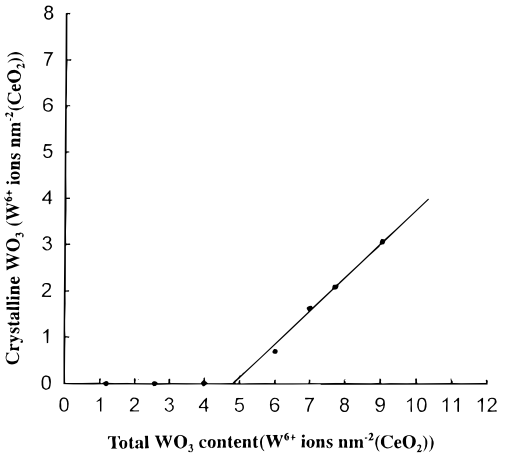

Figure 2. Amount of crystalline WO_3 measured by XRD quantitative analysis versus tungsten oxide content in WO_3/CeO_2 samples.

TABLE 1: Binding Energies of W4f$_{5/2,7/2}$ and Ce3d$_{5/2}$ for Samples with Various WO_3 Loadings

sample number	WO_3 loading (W^{6+} nm^{-2}(CeO_2))	binding energy (eV)		
		W4f$_{5/2}$	W4f$_{7/2}$	Ce3d$_{5/2}$
1	1.2	38.0	36.1	882.6
2	2.6	37.8	35.8	882.1
3	4.0	37.7	35.7	882.7
4	6.2	37.9	35.6	882.9
5	9.0	37.8	35.7	882.9

882.7 eV, respectively. Figure 3 shows the XPS profiles of WO_3, CeO_2, and WO_3/CeO_2 (with a WO_3 loading of 4.0W^{6+} ions nm^{-2}(CeO_2)) samples. The shape of the spectra and the binding energy values of W4f$_{5/2,7/2}$ and Ce3d in the WO_3/CeO_2 sample are the same as those of the corresponding compounds. The results indicate the fact that the dispersion of WO_3 on CeO_2 does not induce any change in the valency of the cations.[22,23] For the supported metal oxide samples, it has been shown that XPS metal-to-support intensity ratios can provide important information regarding the dispersion and crystallite size of the supported metal particles.[24,25] The correlation between the W4f/Ce3d XPS intensity ratio and the loading amount of WO_3 in a series of WO_3/CeO_2 samples is shown in Figure 4. A linear relationship is found for the highly dispersed samples, i.e., line AB. When the loading amount of WO_3 is higher than its dispersion capacity, another straight line, i.e., line BC, shows up; the interception point of the two lines is around 4.8W^{6+} ions nm^{-2} (CeO_2) corresponding to the dispersion capacity of WO_3 on ceria, which is consistent with the value obtained from XRD measurements. The apparently different slopes of the AB and BC straight lines could be understood by taking into consideration the differences on the dispersed states of the supported oxides. It is reasonable to think that for the monolayer-type dispersion of the dispersed W^{6+} species (line AB) the increase in intensity ratio with the increase of WO_3 loading should be faster than that of supported aggregates (line BC). Moreover, it is apparent that when the loading amount of WO_3 exceeds its dispersion capacity the formation of successive uniform overlayers on the top of the monolayer on ceria can be excluded. If this were the case, the overlayers formed by the dispersed tungsten oxide would finally quench the signal of Ce and the intensity ratio of W4f to Ce3d would increase abruptly with the increase of WO_3 loading. As a matter of fact, similar results have been reported in other supported oxide systems, such as, MoO_3/TiO_2,[26] MoO_3/CeO_2,[21] WO_3/Al_2O_3,[22] and V_2O_5/TiO_2,[27,28] etc.

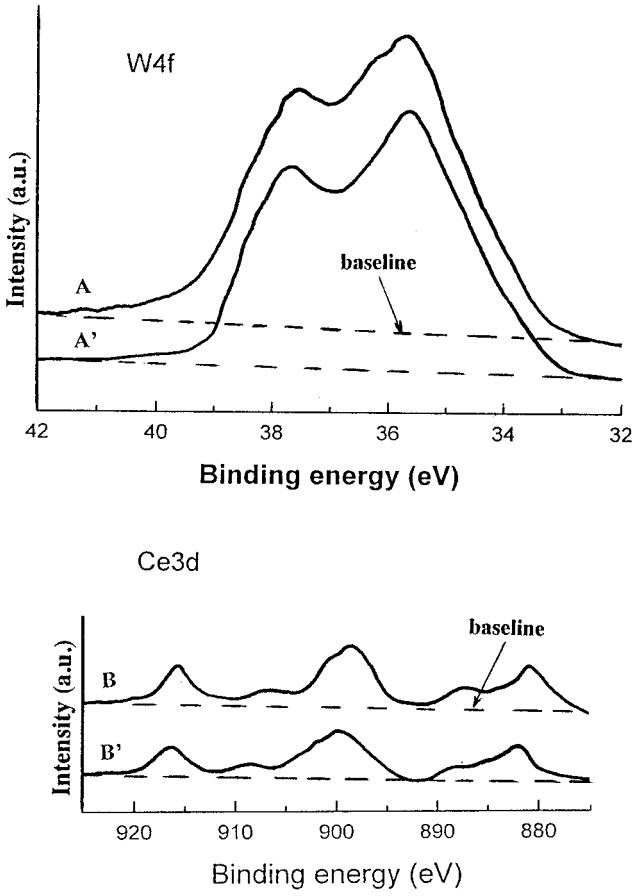

Figure 3. XPS spectra: A, A′ and B, B′ are W4f$_{5/2,7/2}$ and Ce3d spectra of a WO_3/CeO_2 (with WO_3 loading of 4.0 W^{6+} ions nm^{-2}(CeO_2)) and WO_3 and CeO_2 samples, respectively.

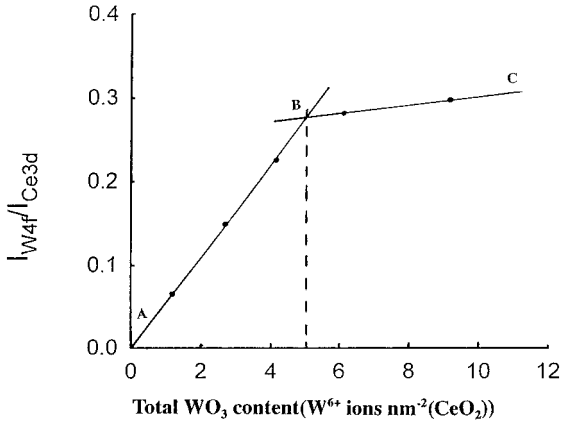

Figure 4. XPS peak intensity ratio I_{W4f}/I_{Ce3d} versus tungsten content in WO_3/CeO_2 samples.

Figure 5 shows representative laser Raman spectra ranging from 600 to 1200 cm^{-1} of WO_3/CeO_2 samples with different WO_3 loadings. Only two peaks at 966 and 802 cm^{-1} are detected in samples with WO_3 loading lower than its dispersion capacity, i.e., 1.2 (a), 2.0 (b), and 3.2 (c) W^{6+} ions nm^{-2}, respectively. For samples with loading higher than the dispersion capacity, i.e., of 5.0 (d) and 9.0W^{6+} ions nm^{-2} (e), two additional sharp bands at 808 and 714 cm^{-1} can be observed due to the formation of bulk WO_3 phase in them. It is noteworthy that the frequencies of the bands at 966 and 802 cm^{-1} do not change with the increase of W loading in samples a−c, i.e., from 1.2 to 3.2 W^{6+} ions nm^{-2}(CeO_2), and the intensity of the band at 966 cm^{-1} also remains almost unchanged in samples with tungsten oxide loading close to or higher than its dispersion capacity as shown

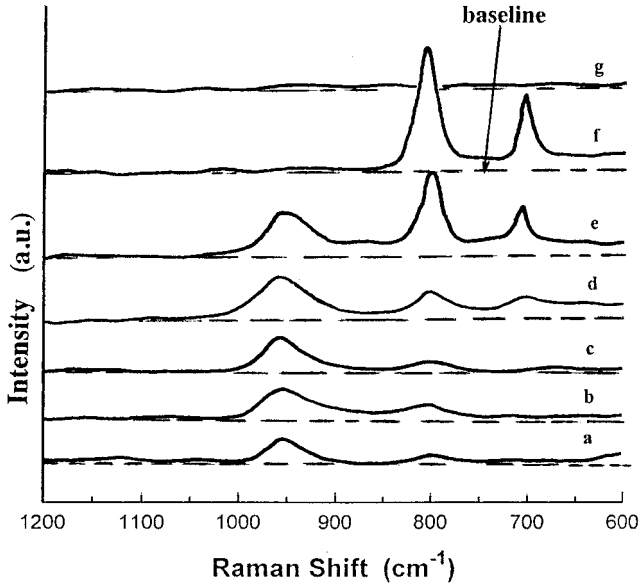

Figure 5. Raman spectra of WO_3/CeO_2 samples with various WO_3 loadings (W^{6+} ions $nm^{-2}(CeO_2)$): (a) 1.2; (b) 2.0; (c) 3.2; (d) 5.0; (e) 9.0; and spectra of WO_3 (f) and CeO_2 (g).

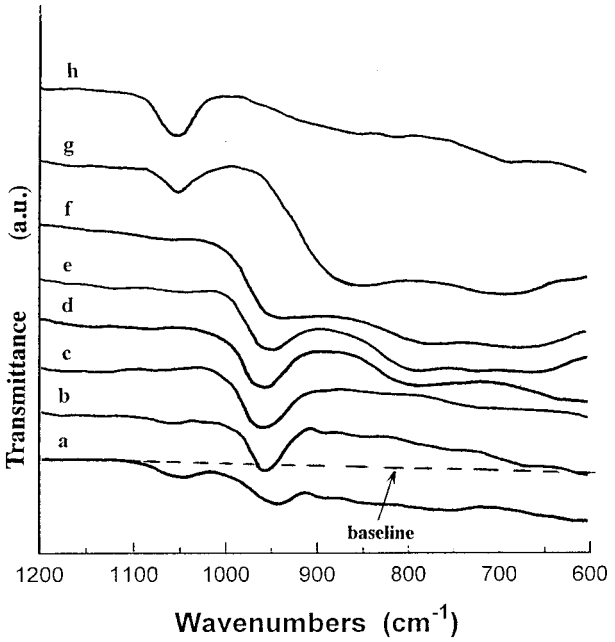

Figure 6. Infrared spectra of WO_3/CeO_2 samples with various WO_3 loadings (W^{6+} ions $nm^{-2}(CeO_2)$): (a) 1.2; (b) 2.0; (c) 3.2; (d) 5.0; (e) 7.2; (f) 9.0; and spectra of a mechanical mixture of WO_3 and CeO_2 (3.0 W^{6+} ions $nm^{-2}(CeO_2)$) (g) and CeO_2 (h).

in spectra d and e. The increase in the intensity of the Raman band around 802−808 cm^{-1} when the loading of WO_3 exceeds its dispersion capacity might be due to the overlapping of bands at 808 cm^{-1} (bulk WO_3) and 802 cm^{-1} (surface tungsten oxide species). The above result is consistent with the conclusion obtained from XRD and XPS studies, i.e., only the highly dispersed tungsten oxide species exist in the low-loading samples and additional bulk WO_3 phase is formed in samples with WO_3 loading higher than their dispersion capacity.

FT-IR spectra of WO_3/CeO_2 samples with different WO_3 loadings are shown in patterns a−f of Figure 6. The spectra of a mechanical mixture of WO_3 and CeO_2 (g) as well as CeO_2 (h) are also presented. For samples with W loading lower than their dispersion capacity, the peak at 965 cm^{-1} is distinct as shown in spectra a−c, and by comparing spectrum a with spectra

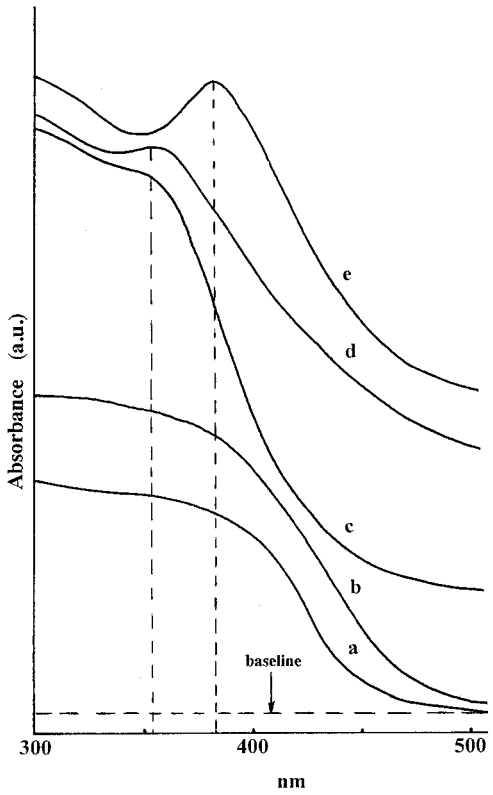

Figure 7. UV-DRS profiles of various samples: (a) CeO_2; (b) WO_3; and WO_3/CeO_2 samples with various WO_3 loadings (W^{6+}ions $nm^{-2}(CeO_2)$) (c) 1.2; (d) 2.0, and (e) 4.6.

g and h, this peak is attributed to the formation of the highly dispersed surface tungsten oxide species. For samples with WO_3 loading higher than their dispersion capacity (d and f), an additional broad peak ranging from 650 to 900 cm^{-1} is attributed to the presence of bulk WO_3, i.e., both the bulk WO_3 and surface tungsten oxide species are existent in these three samples. This conclusion is in good agreement with the results of LRS, XPS, and XRD. Noteworthy, from spectra a−c, the peak intensity at 1060 cm^{-1} relating to the contribution of ceria decreases with the increase of the WO_3 loading, which can be ascribed to the fact that the surface of CeO_2 support was gradually covered by the dispersed tungsten oxide species.

Figure 7 shows the UV-DRS profiles of CeO_2 (a), WO_3 (b), and WO_3/CeO_2 samples with various WO_3 loading (c−e). Apparently, the linkage between the dispersed surface species is enhanced when the loading amount of WO_3 is increased from 1.2 (sample c) to 4.6 (sample e) W^{6+} ions $nm^{-2}(CeO_2)$, i.e., from highly dispersed relatively isolated species to linked "polymerized" species and eventually to species in a close-packed monolayer arrangement. The obvious band shift, i.e., from 365 nm (sample c) to 384 nm (sample d) observed in this region should be attributed to the interaction among the highly dispersed WO_3 species on the surface of CeO_2.

II. A Possible Structure of the Ceria-Supported Tungsten Oxide Species. It has been proven that LRS and FT-IR are powerful and compensative characterization techniques in obtaining detailed information about the structure of supported metal oxides, as each structure is associated with a unique vibrational spectrum. These techniques have been often used to study the state of the dispersed metal oxides, e.g., MoO_3, V_2O_5, WO_3, CrO_3, Nb_2O_5, Re_2O_7, etc., on various supports.[9] The common problem in these studies is the assignment of various bands appearing in the spectra. The complexity comes from the fact that depending on the interaction between the

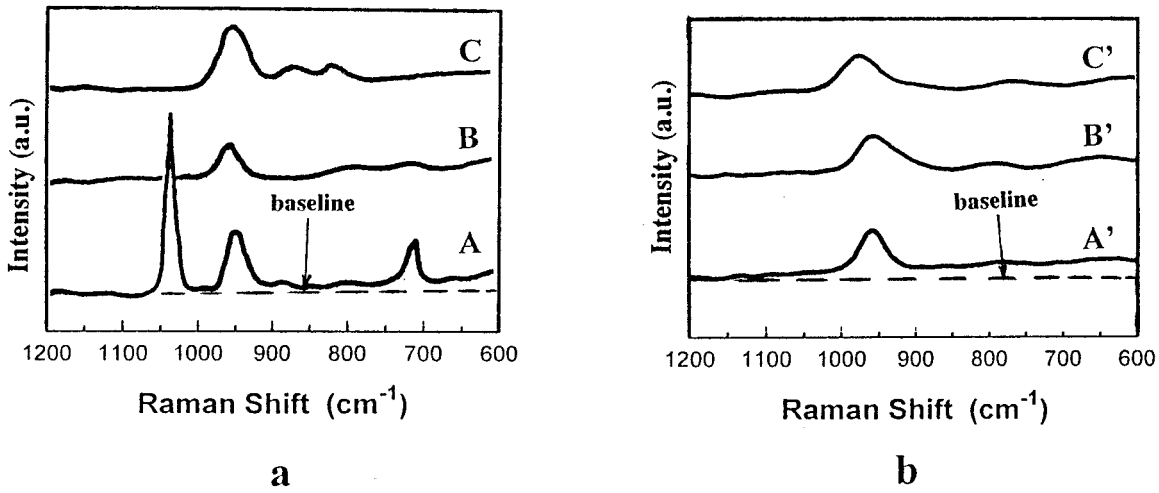

Figure 8. Raman spectra of WO_3/CeO_2 samples ($2.4W^{6+}$ions $nm^{-2}(CeO_2)$): (A) and (B) CeO_2 impregnated with $(NH_4)_6H_2W_{12}O_{40}$ solutions at pH = 3 and 9, respectively, and dried at 373 K for 10 h; (C) CeO_2 impregnated with $(NH_4)_2WO_2S_2$ solution at pH = 9 and dried at 373 K for 10 h. (A′), (B′), and (C′) corresponding to (A), (B) and (C) calcined at 773 K for 2 h, respectively.

dispersed oxide and support as well as the interaction among the dispersed species themselves the dispersed metal oxide might adopt a variety of configurations. Since the general coordinate analysis of surface species is generally impossible under these circumstances, the band assignments are usually made by using model compounds as reference. This method is often used, although it might not provide clear-cut answers due to the complexity of the real systems, for example, the overlapping of the vibrational frequencies associated with various stretching modes of the terminal and bridging metal−oxygen groups.[29]

It is known that by adjusting the pH value of the tungstate solutions the ratio of the WO_4^{2-} and $W_{12}O_{42}^{12-}$ species can be altered. It has been well established that in acidic solutions the predominant species is octahedral $W_{12}O_{42}^{12-}$ ions while the tetrahedral WO_4^{2-} ions are the main species in alkaline and neutral solutions. To get a deeper insight on the nature of the interactions between supported tungsten oxide species and ceria, the structure of surface tungsten species has been investigated for WO_3/CeO_2 samples with the same W loading of $2.4W^{6+}$ ions $nm^{-2}(CeO_2)$ but obtained from different precursors. In short, the samples were prepared by impregnating CeO_2 with solutions of (1) ammonium metatungstate $[(NH_4)_6H_2W_{12}O_{40}]$ at pH = 3, (2) ammonium metatungstate $[(NH_4)_6H_2W_{12}O_{40}]$ at pH = 9, and (3) $(NH_4)_2WO_2S_2$ at pH = 9, respectively.

Samples A, B, and C of Figure 8 were obtained by drying the impregnated samples at 373 K for 10 h, and samples A′, B′, and C′ were obtained by calcining A, B, and C at 773 K for 2 h, respectively.

As can be seen from Figure 8a, the Raman spectra of samples A, B, and C are obviously different, and their differences are attributed to the different precursors used for impregnation, as the low drying temperature has little effect on their structures. It is important to note that calcination has a dramatic effect on the supported tungstates, as shown in Figure 8b, spectra A′, B′, and C′ are similar to new peaks around 965 and 802 cm^{-1} in them. As evidenced by XPS surface analysis, after calcination there are basically no sulfur compounds on the surface of the sample C′. The results point to the fact that the calcination process induced the formation of new surface tungsten oxide species and eliminated the differences of the different precursors because of the strong metal oxide−support interactions. The surface tungsten species obtained after calcination have the same (or similar) chemical state, e.g., a similar coordination environment. The above Raman results for the WO_3/CeO_2 samples are

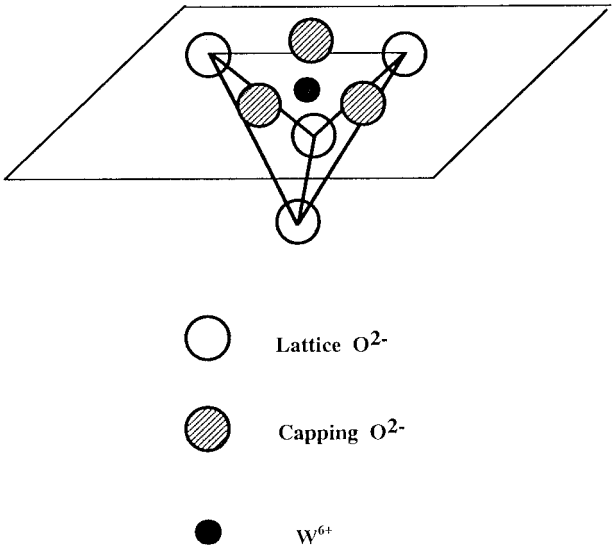

Figure 9. A tentative model of the surface tungsten oxide species formed on the (111) plane of CeO_2 support.

different from those reported by Salvati et al. on the WO_3/Al_2O_3 system.[22] In their work, the doublet at 973 and 333 cm^{-1} was assigned to a tetrahedrally coordinated WO_4^{2-} species and the 973 cm^{-1} band was attributed to the presence of an octahedrally coordinated polymeric tungsten species. The results of our study seem to suggest that the coordination environment of the dispersed tungsten oxide species on ceria is neither octahedrally nor tetrahedrally coordinated, which should have a structure closely related to the surface structure of the ceria support.

It is known that CeO_2 support prepared by calcining $Ce(NO_3)_3{\cdot}6H_2O$ has a fluorite structure with its (111) plane preferentially exposed,[30] and there is mainly only one kind of vacant site, i.e., cubic sites, on the surface of ceria. In contrast, it has been discussed elsewhere that there are two kinds of surface vacant sites, e.g., octahedral and tetrahedral sites, on the preferentially exposed (110) plane of γ-Al_2O_3.[20] According to the incorporation model,[20] the surface tungsten oxide species formed by the incorporation of the W^{6+} ions into the surface of these two supports should be located in entirely different coordination environments. Shown in Figure 9 is the suggested configuration of the surface tungsten oxide species dispersed on CeO_2, which has an asymmetric seven-coordination formed by the incorporation of W^{6+} ions into the surface vacant sites

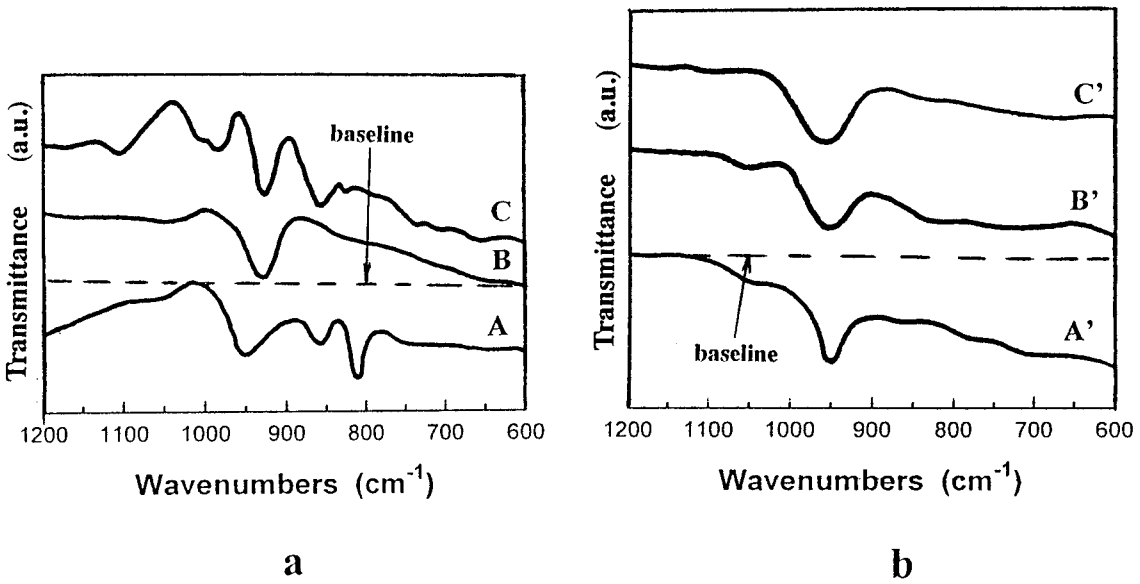

Figure 10. FT-IR spectra of WO_3/CeO_2 samples ($2.4W^{6+}$ ions $nm^{-2}(CeO_2)$). Samples A, B, and C as well as A′, B′, and C′ are the same as those of Figure 8.

of ceria. The FT-IR spectra of the WO_3/CeO_2 samples prepared using the same conditions as mentioned in Raman studies are shown in parts a and b of Figure 10.

The IR spectra A, B, and C of Figure 10a are obviously different because of the different precursors used, and after calcination, the spectra A′, B′, and C′ are similar in having a band near 960 cm^{-1}, as shown in Figure 10b. The IR result is in excellent agreement with that of LRS discussed above, and the same conclusion regarding the role of calcination and the interaction between metal oxide and support can be drawn.

III. TPR and UV-DRS Characterization of WO_3/CeO_2 and CuO/WO_3-CeO_2 Systems. In this section, CeO_2 and WO_3-CeO_2, i.e., CeO_2 premodified with WO_3, samples are designed as supports to explore the importance of the surface of the support on the properties of the dispersed species and the reduction and reflectance spectroscopic properties of various samples are examined. Two WO_3-CeO_2 samples with 1.2 and 4.6 W^{6+} ions $nm^{-2}(CeO_2)$ and BET surface areas of 62 and 54 $m^2\ g^{-1}$, respectively, which were prepared by impregnating CeO_2 with an approximate amount of ammonium metatungstate $[(NH_4)_6H_2W_{12}O_{40}]$ in aqueous solution of at pH = 9, are used as support, followed by drying at 373 K for 10 h and calcining in air at 773 K for 2 h. CuO/WO_3-CeO_2 samples were prepared by impregnating the WO_3-CeO_2 support with aqueous solutions containing the required amount of $[Cu(NH_3)_4]^{2-}$ at pH = 10, followed by drying and calcining under conditions mentioned above.

The reduction properties of CuO supported on CeO_2 and on the WO_3-CeO_2 supports are exmained. The reason for choosing copper oxide as the dispersed species in this study is because generally speaking copper oxide has a relatively lower reduction temperature as compared with those of CeO_2 and WO_3.

TPR results are shown in Figure 11. Profile a reveals that no reduction of bulk WO_3 is observed at temperatures lower than 773 K. Profile b shows the reduction of WO_3-CeO_2 sample with a WO_3 loading of 1.2 W^{6+} ions nm^{-2} (CeO_2); the shoulder peak around 620 K is lower than the initial reduction temperatures of WO_3 (833 K) and CeO_2 (673 K) samples.[31] The above result indicates that the interaction between the surface tungsten oxide and CeO_2 support facilitates the reduction of W^{6+} and/or Ce^{4+} to their lower valence states. The TPR profiles of CuO/CeO_2 with a CuO loading of 5.2 Cu^{2+} $nm^{-2}(CeO_2)$ and CuO

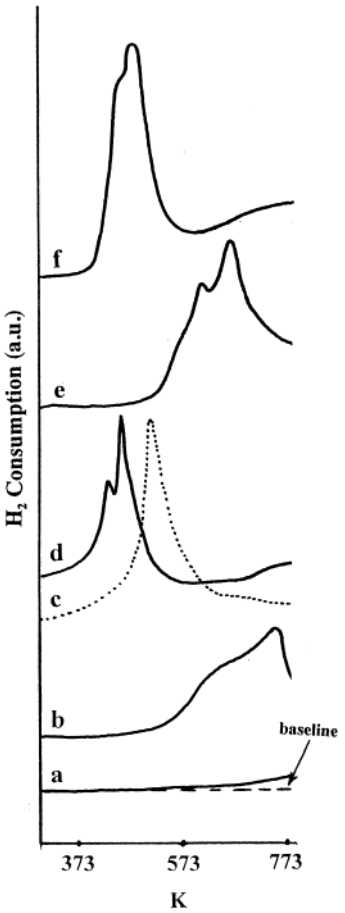

Figure 11. TPR profiles of various samples: (a) WO_3; (b) WO_3/CeO_2 sample with 1.2 W^{6+} ions $nm^{-2}(CeO_2)$; (c) CuO; (d) CuO/CeO_2 sample with 5.2 Cu^{2+} ions $nm^{-2}(CeO_2)$; (e) CuO/WO_3-CeO_2 sample with 5.2 Cu^{2+} ions $nm^{-2}(WO_3-CeO_2)$ and $4.6W^{6+}$ ions $nm^{-2}(CeO_2)$; (f) CuO/WO_3-CeO_2 sample with 5.2 Cu^{2+} ions $nm^{-2}(WO_3-CeO_2)$ and $1.2W^{6+}$ ions $nm^{-2}(CeO_2)$.

samples are also presented for comparison. It has been reported elsewhere that the dispersion of CuO species on ceria facilitates its reduction as compared with that of bulk CuO, and the two reduction peaks at 438 and 446 K are attributed to the stepwise reduction of surface CuO species, i.e., $Cu^{2+} \rightarrow Cu^{+}$ and Cu^{+}

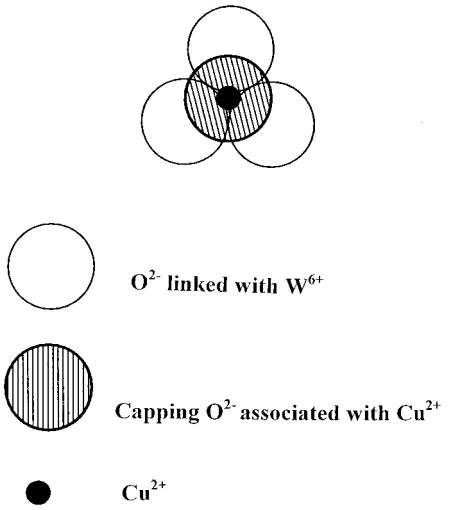

Figure 12. A tentative model of "surface tetrahedrally coordinated Cu^{2+} species" formed on a CeO_2 support premodified with a close-packed monolayer of WO_3.

$\rightarrow Cu^0$.[31,32] Profiles e and f show the reduction of CuO/WO_3-CeO_2 samples with the same Cu^{2+} (5.2 Cu^{2+} ions $nm^{-2}(CeO_2)$) but different W^{6+} loadings (1.2 and 4.6 W^{6+} ions $nm^{-2}(CeO_2)$), respectively. Profiles e and f are apparently different, and they are also different from profile c, i.e., the reduction of copper oxide dispersed on CeO_2 with the absence of WO_3. The results clearly indicate the important role played by the surface of the support on the dispersion states and hence the properties of the supported CuO species. It is argued that when CuO was dispersed on the surface of WO_3-CeO_2 support preloaded with a close-packed monolayer of tugsten oxide, the Cu^{2+} ions might stay on the top of the close-packed oxygen monolayer formed by the oxygen anions accompanying with the incorporated W^{6+} cations. Under such a circumstance, the dispersed copper oxide species might have a tetrahedral coordination environment as schematically shown in Figure 12. The situation on the WO_3-CeO_2 support preloaded with only a small amount of WO_3 is rather different. In such a case, there is no close-packed oxygen monolayer formed on the surface and most of the (111) plane of ceria is still open for the incorporation of the dispersed Cu^{2+} ions. As has been discussed elsewhere, the dispersed Cu^{2+} ions might locate in a five-coordinate environment on the surface of ceria;[31] thus, the five-coordinate and tetrahedral Cu^{2+} species might coexist in the sample, and the ratio of these two species is related to the preloaded amount of WO_3. It seems reasonable to consider that the tetrahedrally coordinated metal oxide species is more stable toward reduction in comparison with the five- or octahedral-coordinated metal cations, as the metal cations are surrounded more closely by the four oxygen anions in the tetrahedral species. An explanation on the different TPR profiles of the three samples can be derived from the above discussion, i.e., the highest reduction temperatures for the tetrahedally coordinated Cu^{2+} cations, profile e, the lowest reduction temperatures for the five-coordinated Cu^{2+} cations, profile d, and intermediate reduction temperatures for the mixture of the five- and tetrahedrally coordinated Cu^{2+} ions, profile f.

UV-DRS has also been used to investigate the interaction among the surface copper oxide and tungsten oxide species as well as the interaction between them and ceria; the results are shown in Figure 13. In comparison with spectrum a (a mechanical mixture of WO_3 and CeO_2), the absorption band around 384 nm in profile b (WO_3/CeO_2) is assigned to the surface WO_3 species formed on CeO_2. For the CuO/WO_3-CeO_2 samples, besides the 384 nm band, one can find new absorption

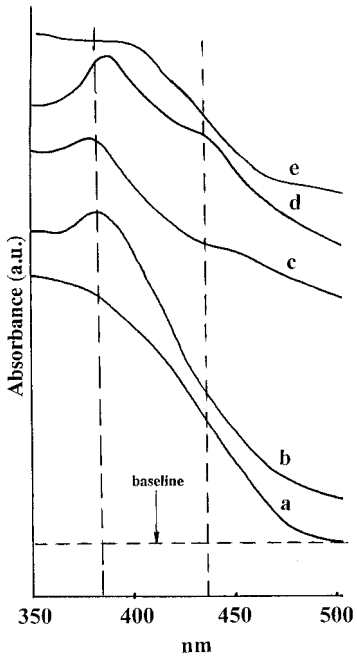

Figure 13. UV-DRS results of various samples: (a) a mechanical mixture of WO_3 and CeO_2 (WO_3/CeO = 1:1,wt %); (b) WO_3/CeO_2 sample with a $4.6W^{6+}$ ions $nm^{-2}(CeO_2)$; (c) CuO/WO_3-CeO_2 sample with 5.2 Cu^{2+} ions $nm^{-2}(WO_3-CeO_2)$ and $1.2W^{6+}$ ions $nm^{-2}(CeO_2)$; (d) CuO/WO_3-CeO_2 sample with 5.2 Cu^{2+} ions $nm^{-2}(WO_3-CeO_2)$ and $4.6W^{6+}$ ions $nm^{-2}(CeO_2)$; (e) CuO/CeO_2 samples with 5.2 Cu^{2+} ions $nm^{-2}(CeO_2)$.

bands around 452 and 438 nm in spectra c and d, respectively; comparatively, spectrum d has a stronger band intensity. Taking into consideration the fact that the preloaded amount of WO_3 ($1.2W^{6+}$ions $nm^{-2}(CeO_2)$) is rather low in sample c, it seems most probable that the dispersed Cu^{2+} ions are mainly incorporated into the surface vacant sites still available on CeO_2. In contrast, for the case of the dispersion of CuO on CeO_2 support preloaded with a close-packed monolayer of WO_3, i.e., sample d, as discussed in the above section, the dispersed CuO species are mainly interacting with the oxygen anion monolayer formed on the top of ceria; thus, the band around 438 nm might relate to the formation of the tetrahedral Cu^{2+} species formed by the interaction between the dispersed CuO and the preloaded WO_3 species.

Conclusion

XRD and XPS data have shown that the dispersion capacity of WO_3 on ceria is about $4.8W^{6+}$ ions $nm^{-2}(CeO_2)$; the result is consistent with the value expected by the incorporation model.

LRS and FT-IR spectra of the WO_3/CeO_2 samples as well as their precursors have shown that an appropriate calcination might eliminate the difference of the precursors and result in the formation of very similar final products. It is suggested that the product is an asymmetric seven-coordinate W^{6+} species formed by the incorporation of W^{6+} ions into the surface vacant sites on the preferentially exposed (111) plane of CeO_2.

TPR and UV-DRS results of WO_3/CeO_2 and CuO/WO_3-CeO_2 samples emphasize the fact that the surface structure of the support has a dramatic influence on the structure and hence the properties of the metal oxide dispersed on it.

Acknowledgment. We thank Dr. Hongwei Hou for providing the $(NH_4)_2WO_2S_2$ sample and acknowledge support from Special Grants for Doctoral Studies, the Ministry of Education,

China as well as grants from the Modern Analytical Center, Nanjing University.

References and Notes

(1) Boehm, H. P.; Knözinger, H. In *Analysis, Science and Technology*; Anderson, J. R., Boudart, M., Eds.; Springer-Verlag: West Berlin, 1983; Vol. 4, p 39.
(2) Yermakov, Yu. I.; Kuznetsov, B. N.; Zakharov, V. A. *Analysis by Supported Complexes*; Elsevier: Amsterdam, 1981.
(3) Delmon, B.; Houalla, M. In *Preparaton of Catalysts II*; Delmon, B., Grange, P., Jacobs, P. A., Poncelet, G., Eds; Elsevier: Amsterdam, 1979; p 447.
(4) Xie Y.; Tang, Y. *Adv. Catal.* **1990**, *37*, 1.
(5) Knöinger, H.; Taglauer, E. In *Catalysis*; Spivey, J. J., Agarwal, S. K., Eds.; A Specialist Periodical Report; The Royal Society of Chemistry: London, 1993; Vol. 10, p 1.
(6) Massoth, F. E. *Adv. Catal.* **1978**, *27*, 265.
(7) Pott, G. T.; Stork, W. H. J. In *Preparaton of Catalysts*; Delmon, B., Jacobs, P. A., Poncelet, G., Eds; Elsevier: Amsterdam, 1976; p 537.
(8) Chianelli, R. R.; Daage, M.; Ledoux, M. J. *Adv. Catal.* **1994**, *40*, 177.
(9) Wachs, I. E. *Catal. Today* **1996**, *27*, 437.
(10) Vuurman, M. A.; Wachs, I. E. *J. Phys. Chem.* **1992**, *96*, 5008.
(11) Dong, L.; Chen, K.; Chen, Y. J. *Solid State Chem.* **1997**, *129*, 30.
(12) Chen, Y.; Dong, L.; Jin, Y.; Xu, B.; Ji, W. In *Studies in Surface Science and Catalysis*; Hightower, J. W., Delgass, W. N., Iglesia, E., Bell, A. T., Eds.; Elsevier Science: New York, 1996; Vol. 101, p 1293.
(13) Trovarelli, A. *Catal. Rev.* **1996**, *38* (4), 439.
(14) Kummer, J. T. *Prog. Energy Combust. Sci.* **1980**, *6*, 177.
(15) Thmas, R.; Moulijn, J. A. *J. Mol. Catal.* **1982**, *15*, 157.
(16) Grange, P. *Catal. Rev—Sci. Eng.* **1980**, *21*, 135.
(17) Matsuoka, Y.; Niwa, M.; Murakami, Y. *J. Phys. Chem.* **1990**, *94*, 1447.
(18) Iwasawa, Y. In *Studies in Surface Science and Catalysis*; Hightower, J. W., Delgass, W. N., Iglesia, E., Bell, A. T., Eds.; Elsevier Science: New York, 1996; Vol. 101, p 21.
(19) Zingg, D. S.; Makovsky, L. E.; Tischer, R. E.; Brown, F. R.; Hercules, D. M. *J. Phys. Chem.* **1980**, *84*, 2898.
(20) Chen, Y.; Zhang, L. F. *Catal. Lett.* **1992**, *12*, 51.
(21) Dong, L.; Chen, Y. *J. Chem. Soc., Faraday Trans.* **1996**, *92* (22), 4589.
(22) Salvati, L.; Makovsky, L. E.; Stencel, J. M.; Brown, F. R.; Hercules, D. M. *J. Phys. Chem.* **1981**, *85*, 3700.
(23) Normand, F. Le, Hilaire, L.; Kili, K.; Krill, G.; Maire, G. *J. Phys. Chem.* **1988**, *92*, 2561.
(24) Kerkhof, F. P. J. M.; Moulijn, J. M. *J. Phys. Chem.* **1979**, *83*, 1612.
(25) Fung, S. C. *J. Catal.* **1979**, *58*, 454.
(26) Gui, L.; Liu, Y.; Guo, Q.; Huang, H.; Tang, Y. *Chin. Sci. B* **1985**, *6*, 509.
(27) Bond, G. C.; Zurita, J. P.; Flamerz, S. *Appl. Catal.* **1986**, *27*, 353.
(28) Vuurman, M. A.; Wachs, I. E.; Hirt, A. M. *J. Phys. Chem.* **1991**, *95*, 9928.
(29) Cotton, F. A.; Wang, R. M. *Inorg. Chem.* **1965**, *4*, 867.
(30) Cochrane, H. D.; Hutchison, J. L. *Ultramicroscopy* **1989**, *31*, 138.
(31) Dong, L.; Jin, Y. S.; Chen, Y. *Sci. China, Ser. B* **1997**, *40* (1), 24.
(32) Hurst, N. W.; Gentry, S.; Jone, A. *Catal. Rev—Sci. Eng.* **1982**, *24* (2), 233.